

## Original Research

# Diffusion-Weighted MRI for Monitoring Tumor Response to Photodynamic Therapy

Hesheng Wang, MS<sup>1,2</sup> and Baowei Fei, PhD, EngD<sup>1,3\*</sup>

**Purpose:** To examine diffusion-weighted MRI (DW-MRI) for assessing the early tumor response to photodynamic therapy (PDT).

**Materials and Methods:** Subcutaneous tumor xenografts of human prostate cancer cells (CWR22) were initiated in athymic nude mice. A second-generation photosensitizer, Pc 4, was delivered to each animal by a tail vein injection 48 h before laser illumination. A dedicated high-field (9.4 Tesla) small animal MR scanner was used to acquire diffusion-weighted MR images pre-PDT and 24 h after the treatment. DW-MRI and apparent diffusion coefficients (ADC) were analyzed for 24 treated and 5 control mice with photosensitizer only or laser light only. Tumor size, prostate specific antigen (PSA) level, and tumor histology were obtained at different time points to examine the treatment effect.

**Results:** Treated mice showed significant tumor size shrinkage and decrease of PSA level within 7 days after the treatment. The average ADC of the 24 treated tumors increased 24 h after PDT ( $P < 0.001$ ) comparing with pre-PDT. The average ADC was  $0.511 \pm 0.119 \times 10^{-3} \text{ mm}^2/\text{s}$  pre-PDT and  $0.754 \pm 0.181 \times 10^{-3} \text{ mm}^2/\text{s}$  24 h after the PDT. There is no significant difference in ADC values pre-PDT and 24 h after PDT in the control tumors ( $P = 0.20$ ).

**Conclusion:** The change of tumor ADC values measured by DW-MRI may provide a noninvasive imaging marker for monitoring tumor response to Pc 4-PDT as early as 24 h.

**Key Words:** diffusion-weighted MRI; prostate cancer; photodynamic therapy; apparent diffusion coefficients (ADC); efficacy assessment; treatment monitoring

**J. Magn. Reson. Imaging 2010;32:409–417.**

© 2010 Wiley-Liss, Inc.

PHOTODYNAMIC THERAPY (PDT) is an emerging therapy that has shown promise for treating various cancers in both preclinical and clinical studies (1). PDT uses laser light with appropriate wavelength to activate preadministered tumor-localized photosensitizer. With oxygen presence, the activation of the photosensitizer generates singlet oxygen species that react with cellular structure and effectively ablate tumors either through direct cell destruction or local vasculature damage (2). PDT can be localized at planned regions, consequently minimizing injury to the surrounding normal tissue. PDT with different photosensitizer drugs has shown potentials for treating a variety of cancers including prostate cancer (3–6).

PDT effect is determined by several parameters that include drug choice, drug dose, light dose, light delivery rate, and light delivery pattern. It is valuable if a technique can be used to monitor the tumor response to PDT and predict treatment efficacy at an early time; thereby, immediate prognosis and early consideration of adjuvant treatment are allowed. Traditionally, treatment efficacy assessment was determined by the variation of tumor size and thus may require weeks or months after therapy. Noninvasive imaging such as MRI can provide in vivo information about tissue physiology and morphology, whereby allow assessment of the tumor response by monitoring the change of treatment-induced tissue properties.

A variety of MRI techniques have also been studied for assessing tumor response to PDT. MRI was used to study the therapeutic effect of PDT in normal rat brain (7). It has been shown that both T1 (8,9) and T2 values (6,8) increased after PDT. High-field MRI has been used to evaluate PDT-induced treatment effect (6,10). Gadolinium contrast-enhanced MRI revealed a decrease of tissue perfusion 5 h after PDT in rat borne tumors (11) and detected vascular lesion formation of recurrent prostate tumors 7 days after PDT (12). One week after the vascular-targeted PDT of locally recurrent prostate tumors (13), Gd contrast-

<sup>1</sup>Emory Center for Systems Imaging, Department of Radiology, Emory University, Atlanta, Georgia, USA.

<sup>2</sup>Department of Biomedical Engineering, Case Western Reserve University, Cleveland, Ohio, USA.

<sup>3</sup>Department of Biomedical Engineering, Emory University and Georgia Institute of Technology, Atlanta, Georgia, USA.

Contract grant sponsor: National Cancer Institute; Contract grant number: R21CA120536, R24CA110943; Contract grant sponsors: Atlanta Clinical and Translational Science Institute and Georgia Cancer Coalition (Distinguished Clinicians and Scientists Award; PI, Fei).

\*Address reprint requests to: B.F., Emory Center for Systems Imaging, Department of Radiology, Emory University, 1841 Clifton Road NE, Atlanta, GA 30329. E-mail: fei@emory.edu

Received December 15, 2009; Accepted April 29, 2010.

DOI 10.1002/jmri.22247

Published online in Wiley InterScience (www.interscience.wiley.com).

enhanced MRI depicted irregular margins of the therapeutic effect. Blood oxygenation level-dependent (BOLD) contrast MRI was applied to monitor PDT in a solid tumor model (14), where 25–40% BOLD signal attenuation was detected in the treated tumors. Another MRI technique of  $^{31}\text{P}$  MR spectroscopy (MRS) was used to image zinc phthalocyanine-based PDT of RIF-1 murine fibrosarcoma in mice (15).  $^{19}\text{F}$  MRS was also applied to study the pharmacokinetic profile of a fluorinated photosensitizer in a RIF tumor model (16).

Diffusion weighted MRI (DW-MRI) detects displacement of water molecules and several studies have demonstrated its potential for monitoring tumor response to PDT. A biphasic change in the apparent diffusion coefficient (ADC) derived from DW-MRI has been reported within the first 24 h after TOOKAD-based PDT of prostatic adenocarcinoma in mice (17). Another TOOKAD-PDT study found a markedly decrease of ADC values in the necrotic regions 7 days after PDT in a normal canine prostate model (18). DW-MRI with high-b-value shows potentials for predicting treatment outcome in a study of PDT of colon carcinoma in mice (19).

Both MRI and positron emission tomography (PET) have been used to study the tumor response to Pc 4-PDT (6,20,21). Assessment of therapeutic effect was improved by fusion of MRI anatomical and PET functional information (22). We are developing noninvasive imaging and quantitative analysis techniques to identify potential biomarkers of early tumor response to PDT. In present study, we evaluate the capability of DW-MRI for identifying early therapeutic efficacy of Pc 4-PDT in a CWR22 human prostate cancer model. CWR22 is androgen dependent and prostate specific antigen (PSA) level can be measured as an independent parameter of therapeutic efficacy. This study suggests that the change of tumor ADC in response to Pc 4-PDT could eventually be useful for monitoring Pc 4-PDT of prostate cancer in the clinic.

## MATERIALS AND METHODS

### Animal Tumor Model

An androgen-dependent prostate tumor xenograft model CWR22 was originally derived from a primary human prostatic carcinoma (23). The frozen CWR22 cancer cells were thawed in  $37^{\circ}\text{C}$  water, washed with tissue culture medium (RPMI 1640, Hyclone Laboratories, Inc., Logan, UT) with 20% calf serum (Hyclone Laboratories, Inc., Logan, UT), and then filtered through a single layer of Nitex with  $100\ \mu\text{m}$  porosity (Tetko, Inc., Briarcliff Manor, NY). The cells were suspended in Matrigel (BD Biosciences, Bedford, MA) with a volume of at least equal to the cell volume. The suspension was draw into 1.0-cc syringes with 19-gauge needles for 0.2 mL volume per injection. Athymic nude mice of 4–8 weeks old were housed under controlled conditions (12 h dark and light cycles;  $20\text{--}24^{\circ}\text{C}$  temperature) and with freely reachable sterilized mouse chow. A 12.5-mg sustained-release testosterone pellet (Innovative Research of America, Sarasota, FL) was planted in each nude mouse 1 week before

cell injection. Each animal was given an injection of cell suspension subcutaneously on the other side of the implanted testosterone and far from the lung and heart to minimize motion effect in imaging.

The animal experiments were approved by the Institutional Animal Care and Use Committee (IACUC) and conformed to the guidelines of the National Institutes of Health for the care and use of laboratory animals.

### Photosensitizer Formation

A photosensitizing drug, the silicon phthalocyanine Pc 4,  $[\text{HOSiPcOSi}(\text{CH}_3)_2(\text{CH}_2)_3\text{N}(\text{CH}_3)_2]$  was used in our study (24). Stock solution (1 mg/mL) was prepared by 50% Cremophor EL and 50% absolute ethanol, and then diluted with nine volumes of normal saline. For treatment, Pc 4 solution was administered with concentration of 0.05 mg/mL (0.07 mM) obtained by further mixing the solution with an equal volume of 5% cremophor EL, 5% ethanol, and 90% saline.

### PDT Protocol

PDT was performed when the subcutaneous tumors reaching 8–10 mm in diameters (typically in 2–4 weeks). The mouse was constrained and injected with 0.6 mg/kg Pc 4 dose (e.g., 240  $\mu\text{L}$  to a 20 g mouse) intravenously by means of the tail vein. The dose was found to be optimal for tumor treatment in a xenograft model of OVCAR-3 ovarian epithelial carcinoma (25) and was also used in an early study (6). Treatment and imaging of the animals were performed in a small-animal imaging facility 48 h after the Pc 4 injection. For PDT, the tumor was illuminated for 25 min with light of a  $150\ \text{J}/\text{cm}^2$  fluence and  $100\ \text{mW}/\text{cm}^2$  irradiance using a diode laser (Applied Optonics Corp., Newport, CT). The light was delivered with a wavelength of 672 nm at which Pc 4 obtains maximal absorption. The light was adjusted to illuminate the whole tumor and spare the surrounding skin which was covered with black tapes to avoid possible damage. A total of 24 tumor-bearing mice were treated and imaged in this study. Two types of control experiments were also conducted. One was the light control ( $n = 3$ ), in which the tumors were illuminated by laser light excluding Pc 4 injection; the other was the dark control ( $n = 2$ ), in which the mice had Pc 4 injection but were not irradiated with laser light. All parameters for the control mice were same as those used in the PDT-treated mice. Serum PSA levels and tumor sizes were measured at different time points after treatment.

### MR Imaging

Animals were imaged using a dedicated whole body mouse coil in a high-field (9.4T) small animal scanner (Bruker BioSpin GmbH, Rheinstetten, Germany). The mouse was continuously supplied with 2% isoflurane (EZAnesthesia, Palmer, PA) in air for anesthetization. Animals' respiration rate and body temperature were monitored throughout the entire imaging. The body temperature typically was maintained between  $35^{\circ}\text{C}$

and 37°C using a feedback system that blew warm air to the mouse by means of a plastic pipe. The respiration was manually controlled by adjusting the isoflurane rate. MR acquisition was triggered by the respiration signal to minimize motion effect. Therefore, one respiration period needs to be long enough for a complete MR signal acquisition defined by the parameter of time to repetition (TR). We maintained a mouse respiration rate of no more than 40 per min, which allowed maximal TR around 1500 ms. As DW-MRI is sensitive to body motion, the respiration triggering was important for MR image acquisitions.

Before the DW-MRI scan, a coronal scout image was obtained to determine position and size of the tumors. A diffusion gradient linearly incremented in the range of 0 to 400 mT/m with  $\Delta = 35$  ms and  $\delta = 3$  ms yielded five  $b$  values (16.5, 133.35, 409.269, 759.643, 985.108 s/mm<sup>2</sup>), thereby, to generate diffusion-weighted MRI and enable ADC calculation. ADC was measured along a single direction assuming water diffusion in the tumor is isotropic. The other parameters for MR image acquisition were TR = 1282 ms, echo time (TE) = 52.5 ms, field of view: 3.5 cm × 3.5 cm, matrix size: 128 × 128, slice thickness: 0.5 mm, receiver bandwidth: 25,000 Hz, and no average. The total number of slice depended on the tumor size. Typically, 15–20 coronal slices were acquired to cover the whole tumor. The total DW-MRI scan time was around 15 min. Each mouse was scanned before, immediately after, and 24 h after PDT to characterize the tumor response to Pc 4-PDT.

### MRI Data Analysis

We used the software package Paravision 3.1 (Bruker BioSpin GmbH, Rheinstetten, Germany) for ADC computation. The ADC was calculated by a linear least square fitting of the 5  $b$  MR signals to monoexponential decay at each voxel, which is denoted as:

$$S = S_0 \exp(-b * ADC) \quad [1]$$

$S_0$  and  $S$  are proton signal intensities without and with the presence of diffusion-sensitizing gradient, respectively. ADC is apparent diffusion coefficient that characterizes the water diffusion at the location.  $b$  is the diffusion weighting factor and is determined by the imaging parameters setting according to [26]:

$$b = \gamma^2 G^2 \delta^2 \left( \Delta - \frac{\delta}{3} \right) \quad [2]$$

$G$  is the gradient pulse strength,  $\delta$  is the gradient pulse duration,  $\Delta$  is separation time of gradient pulses, and  $\gamma$  is the gyromagnetic ratio that is a constant for a nucleus.

We manually segmented the tumors slice by slice from the DW-MRI using the image analysis software, Analyze (AnalyzeDirect, Inc., Overland Park, KS). The tumor boundary was manually drawn on the MR images and was then saved as an object map. The tumor boundary was copied to the ADC map to calculate the statistical properties (e.g., mean, standard

deviation, and histogram) of the ADC values within the tumor.

### Histologic Analysis

To measure tumor response histologically, seven mice in the treated group and two controls were euthanized 24 h after PDT. The tumors were dissected and prepared for histological slides. The tissue preparation for histology was described by Fei et al (6). After being quickly removed from the body, the tumor was fixed in a large volume of 10% formalin for 1 h; and tumor was then cut into 3- to 5-mm-thick slices along the approximately same orientation as the coronal direction in which MR images were acquired. Typically two to four slices were obtained for each tumor. The slices were placed into cassettes and were fixed in 10% formalin for at least 24 h to allow complete tissue fixation. Usually, one to two histological sections with 3  $\mu$ m thickness for each tissue slice were obtained and stained with hematoxylin and eosin (H&E). The sections were examined using a light microscope (BX40, Olympus, Japan) and then digitalized by a motorized system (ProScan, Prior Scientific, Rockland, MA) to acquire color histological images.

### PSA Measurement

Blood samples (0.1 mL) were collected from the mouse tail to measure serum PSA level before, 24 h, and 7 days after PDT. The blood samples were centrifuged for 10 min at 5000–5500 RPM to separate the blood into red blood component and blood serum. The serum was sent to the clinical lab at the University Suburban Health Center (Cleveland, Ohio) for PSA measurement.

### Statistical Analysis

The ADC values of tumors at the three time points (pre-PDT, immediately after PDT, and 24 h after PDT) were analyzed statistically. A two-tailed two-sample student's  $t$ -test in Microsoft Excel 2007 (Microsoft, Seattle, WA) was used to test the difference of tumor ADCs at the three time points. Statistical significance was defined by a  $P$  value of 0.05.

### DW-MRI Image Classification

A multivariate image classification algorithm called multi-scale fuzzy  $c$ -means method was applied to classify DW-MRI and ADC maps of the treated tumor into necrotic and viable regions. The classification method has been validated in an early study (27). Based on the two-element vector consisting of DW-MRI intensity and ADC value, the classification method assigned a tissue type (viable or necrotic) for each voxel within the segmented tumor. The classification result provides the distribution information of necrotic tissue within a treated tumor as a measurement for treatment effect.

Histology was used as the gold standard to validate the measurements from the MR images. The digitized,

high-resolution histologic images were down sampled to a pixel resolution of 0.1 mm. We manually segmented the tumor region and excluded the no-tumor tissues on the histologic images. Necrotic regions were manually drawn within the segmented tumor. Because we carefully maintained the tumor orientation during the dissection and because the tumor was cut along approximately the same coronal direction, the histologic slide from the tumor center was aligned with the center slice in tumor MR images.

## RESULTS

Figure 1 shows the diffusion weighted MR images and the corresponding ADC maps of a treated CWR22 mouse pre- and 24 h post-PDT with corresponding images from a control mouse in Figure 2. In the treated mouse, an ADC increase within the tumor with surrounding edema is seen, which did not occur in the control animal. The tumor ADC values increased 24 h after PDT, indicating higher water diffusivity compared with pre-PDT. Edema was observed surrounding the tumor immediately after the treatment and lasted for a few days, which was shown by the bright region in the ADC map 24 h after PDT. However, the ADC map did not show visible intensity change between pre-PDT and 24 h after PDT. Edema or fluid swelling was not observed in the images.

Figure 3 shows the ADC histograms of tumors pre-PDT and 24 h after PDT. A histogram of tumor ADC

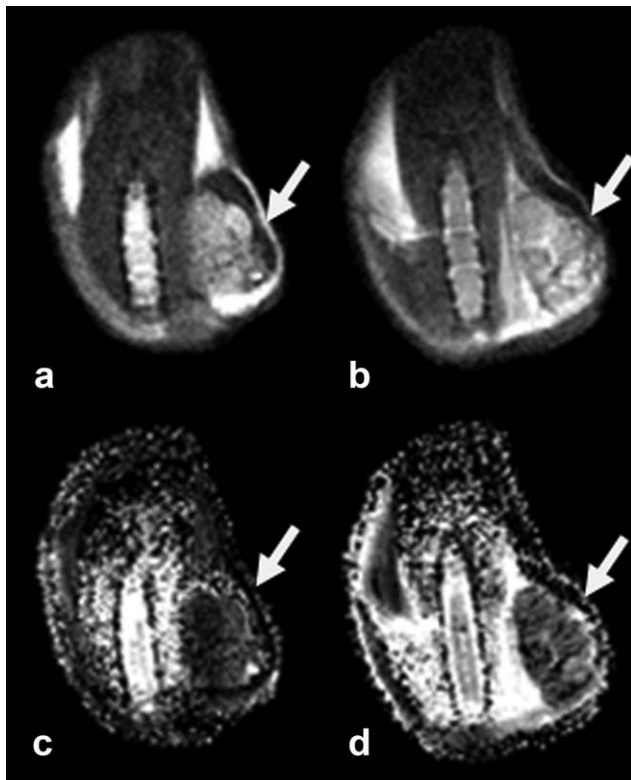


**Figure 1.** DW-MRI image and ADC map of a treated mouse pre-PDT and 24 h after PDT. **a,b:** The MR images of the treated mouse pre-PDT and 24h after PDT. **c,d:** The corresponded ADC maps for the two MR images. The tumor was shown by the arrows.



**Figure 2.** DW-MRI image and ADC map of a control mouse. **a,b:** The MR images of a light control mouse (having laser illumination but without Pc 4 injection) before light illumination and 24 h later. **c,d:** The corresponded ADC maps for the two MR images. The tumor was shown by the arrows.

map plots the number of tumor voxels at each ADC value. It was generated by counting the voxel number versus discrete ADC value with a level of  $4 \times 10^{-5}$   $\text{mm}^2/\text{s}$ , which showed the main trend of ADC distribution and minimized noise fluctuation. For the treated tumor (Fig. 3a), the ADC histogram 24 h after PDT was shifted to the right relative to the one pre-PDT, indicating the increase of tumor ADC values 24 h after treatment. The average ADC was  $0.405 \times 10^{-3}$   $\text{mm}^2/\text{s}$  pre-PDT and was  $0.686 \times 10^{-3}$   $\text{mm}^2/\text{s}$  24 h after PDT. However, the light control (Fig. 3b) and the dark control tumor (Fig. 3c) did not show substantial change in the ADC histogram 24 h after PDT. The light control tumor had an average ADC of  $0.772 \times 10^{-3}$   $\text{mm}^2/\text{s}$  pre-PDT and  $0.759 \times 10^{-3}$   $\text{mm}^2/\text{s}$  24 h after PDT. The dark control tumor had an average ADC of  $0.454 \times 10^{-3}$   $\text{mm}^2/\text{s}$  at pre-PDT and  $0.461 \times 10^{-3}$   $\text{mm}^2/\text{s}$  24 h later. We did not observe a shift of ADC histograms between pre-PDT and immediately after PDT for both the treated and control tumors.

ADC values significantly increased for treated tumors and the changes were not observed in control animals. A total of 24 CWR22 tumor-bearing mice were treated and imaged in the study. The five control mice were also imaged and analyzed with the same protocol. Figure 4 compared the average ADC of 24

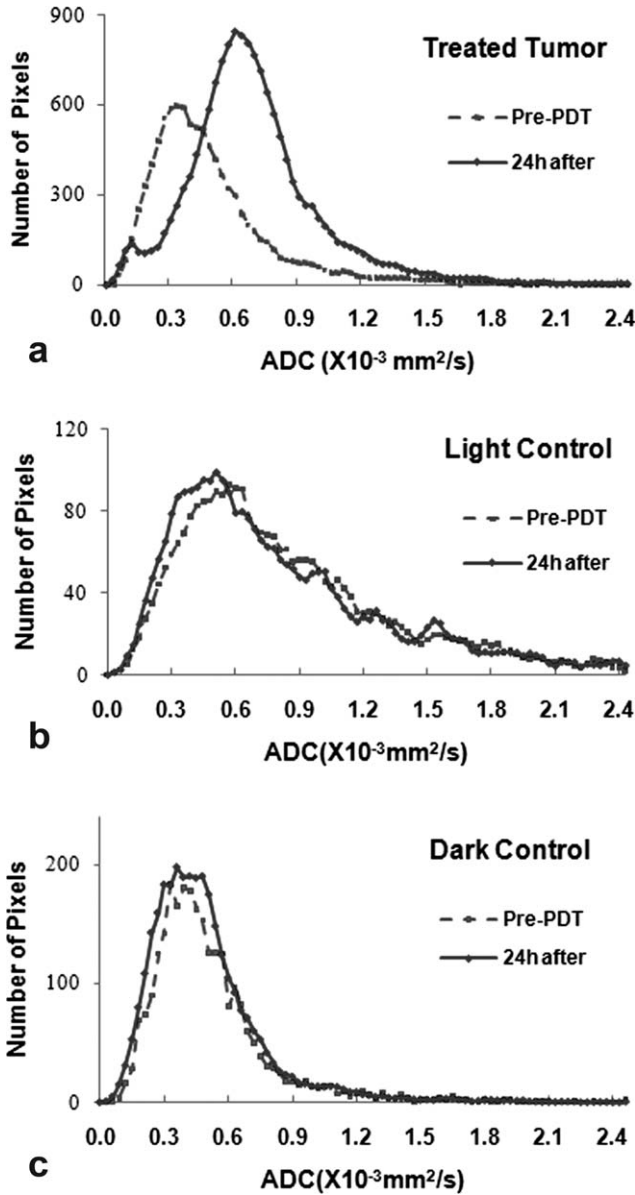


**Figure 3.** Histograms of tumor ADC values in treated and control tumors. **a:** A treated tumor. **b:** A light control tumor (with light illumination but without Pc4 drug). **c:** A dark control tumor (without light illumination but with Pc4 drug).

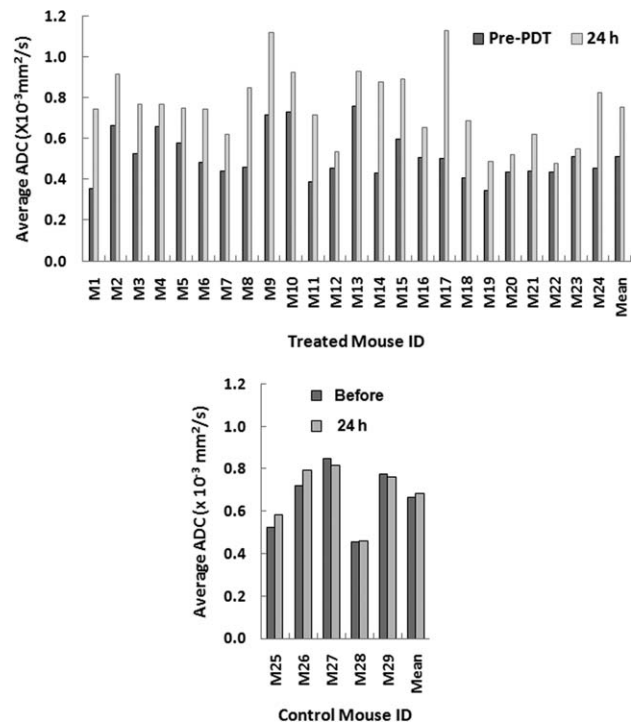
treated tumors and 5 controls between pre-PDT and 24 h after PDT. There was a consistent increase of average ADC in the treated tumors 24 h after PDT compared with the value pre-PDT. The average ADC values for the treated mice were  $0.511 \pm 0.119 \times 10^{-3} \text{ mm}^2/\text{s}$  pre-PDT and  $0.754 \pm 0.181 \times 10^{-3} \text{ mm}^2/\text{s}$  24 h after PDT. A student's paired t-test showed a significant increase of ADC values ( $P < 0.001$ ) 24 h after PDT with respect to pre-PDT. For the controls, no significant ADC change between the two time points were observed. The mean ADC of the 5 control tumors were  $0.664 \pm 0.168 \times 10^{-3} \text{ mm}^2/\text{s}$  pre-PDT and  $0.683 \pm 0.154 \times 10^{-3} \text{ mm}^2/\text{s}$  24 h after PDT ( $P = 0.20$ ).

Figure 5 shows the tumor volumes of 15 treated tumors and 5 controls pre-PDT and 7 days after PDT.

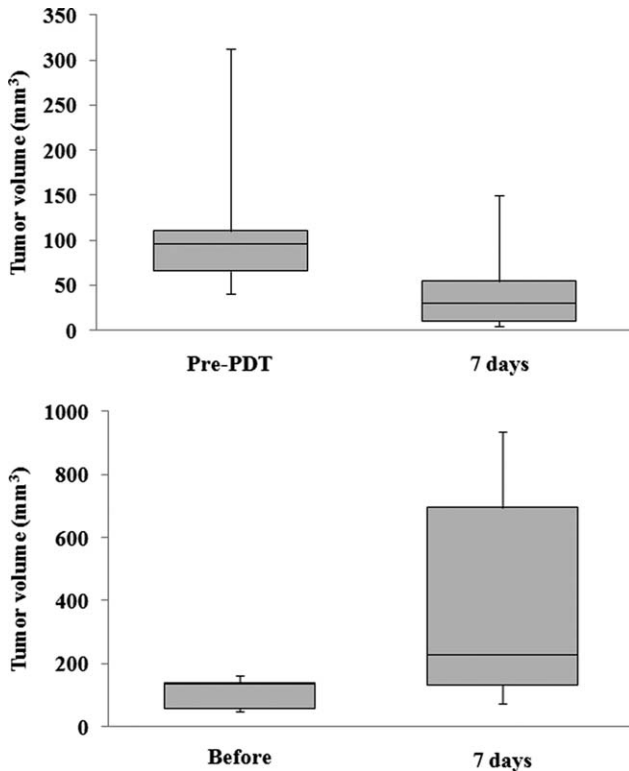
The tumor volume was measured by a caliper and was calculated as  $0.5 \times \text{width} \times \text{length} \times \text{height}$ . The average tumor size of treated tumors shrunk from  $136.7 \pm 26.5 \text{ mm}^3$  pre-PDT to  $57.5 \pm 18.7 \text{ mm}^3$  7 days after the treatment. In contrast, the control tumor volumes increased from  $109.3 \pm 23.3$  pre-PDT to  $412.8 \pm 170.5 \text{ mm}^3$  7 days later.

Figure 6 shows the PSA level of the 15 treated and 5 control mice. The average PSA level of treated mice decreased from  $27.9 \pm 5.6 \text{ ng/mL}$  pre-PDT to  $7.2 \pm 2.2 \text{ ng/mL}$  7 days after PDT. However, the average PSA level of controls increased from  $24.9 \pm 6.4 \text{ ng/mL}$  pre-PDT to  $97.5 \pm 45.1 \text{ ng/mL}$  7 days after PDT. PSA level of control mice continuously increased until the tumor size reached the endpoint when the mouse was euthanized.

Figure 7 shows typical histologic slides of treated and control tumors. Edema surrounding the treated tumor was visible in the histologic image. For the treated tumor, the histologic slide shows broken cells, cell debris, increased intercellular space, and necrotic subregions. On the contrary, the histologic slide of the control tumor shows that the integrated tumor cells were densely distributed. Substantial variation of histological appearance was also observed in the treated tumor, which was consistent with intensity variations in DW-MRI images and ADC maps. On histologic images, viable tumor has cells with well-defined cell



**Figure 4.** Average ADC values within segmented tumors pre-PDT and 24 h after PDT for 24 treated mice and 5 control mice. **Top:** The average tumor ADC values increased 24 h after PDT compared with pre-PDT in 24 treated mice. **Bottom:** The average ADC values of control tumors pre-PDT and 24 h after PDT. M27 and M28 were dark controls. M25, M26, and M29 were light controls. No significant ADC change between pre-PDT and 24 h after PDT were observed for the control tumors.



**Figure 5.** Tumor volumes pre-PDT and 7 days after PDT for the 15 treated tumors (**top**) and 5 control tumors (**bottom**). The tumor volumes decreased 7 days after PDT in the treated group. However, the control group had increased tumor volumes 7 days later compared with pre-PDT. The box-and-whisker plot shows minimum, lower quartile, median, upper quartile, and maximum.

borders and nuclei that are intact with coarse chromatin. Necrotic tumor demonstrates cell shrinkage, disappearing cell membranes and fragmented nuclei. The cell morphologic change such as broken cells would lead to the change of water diffusion within the tumor and thus provides the mechanism for diffusion-weighted MRI to detect the early tumor response by measuring the change of tissue water diffusion.

Figure 8 showed a typical classification result from a middle MR image slice of a treated tumor. The histological image of the same tumor was also classified into the viable and necrotic classes. The focal necrotic region was indicated with the absence of nuclei. The similarity between MRI classification and histologic delineation shows the effectiveness of quantifying tumor tissue by noninvasive MR imaging. The correlation between MRI classification and histology segmentation was shown in Figure 9. An excellent correlation was seen between MRI classification and histology segmentation ( $R^2 = 0.977$  from 20 tumor slices) and between the ratio of viable region with respect to the whole tumor on both MRI and histology ( $R^2 = 0.899$ ).

## DISCUSSION

This study demonstrates that DW-MRI and ADC can effectively detect tumor response to Pc 4-PDT as early

as 24 hours after treatment. Using a CWR22 prostate tumor model, this study shows significant rising of water molecule diffusion 24 h after Pc 4-PDT. The change in ADCs is consistent with the treatment effect characterized by the change in tumor sizes and PSA level 7 days after therapy. The finding suggests that measurement of tumor ADC change may provide a useful tool to monitor the early tumor response and to determine the effectiveness of the therapy. The ADC study is consistent with an early report that shows PDT-introduced change in T2 values 24 h after PDT in a PC-3 tumor model (6). The changes in T2 values may also relate to alteration of water content result from the treatment. In addition to MRI methods, PET can detect tumor metabolic changes 24 h after PDT, as reported by Fei et al (20,22).

The MR image classification result was correlated well with histologic findings. The relationship between image classification and histological measurement indicates that MR image classification might reveal the spatial distribution of the treatment effect and thus provides regional measurement for therapy assessment. PDT ablates tumors through the interaction of light, photosensitizer, and oxygen. Any inhomogeneity of light transmission, photosensitizer distribution, oxygen availability, and tissue microenvironment could induce the heterogeneity of intratumor response. The heterogeneity may be quantified by

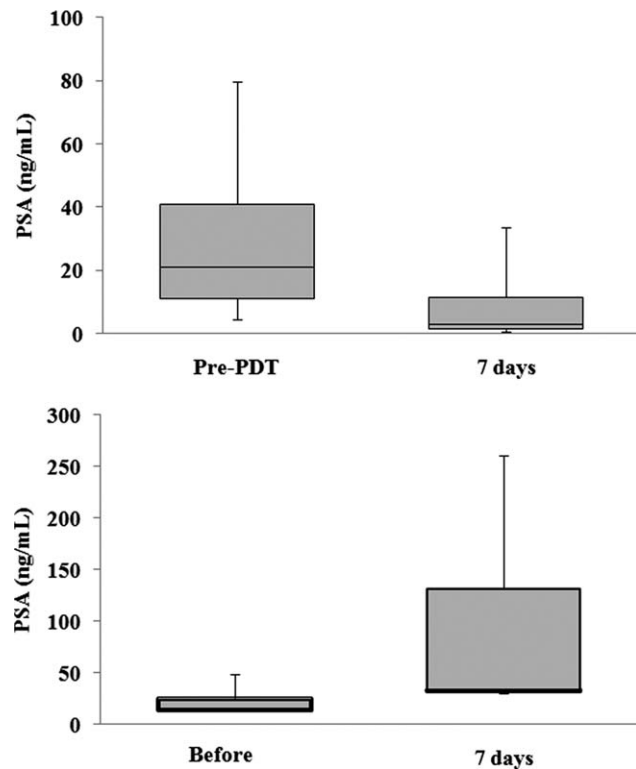


**Figure 6.** PSA level pre-PDT and 7 days after PDT in 15 treated mice (**top**) and 5 control animals (**bottom**). The PSA level decreased in the treated mice. In the control mice, the PSA increased 7 days later. The box-and-whisker plot shows minimum, lower quartile, median, upper quartile, and maximum.

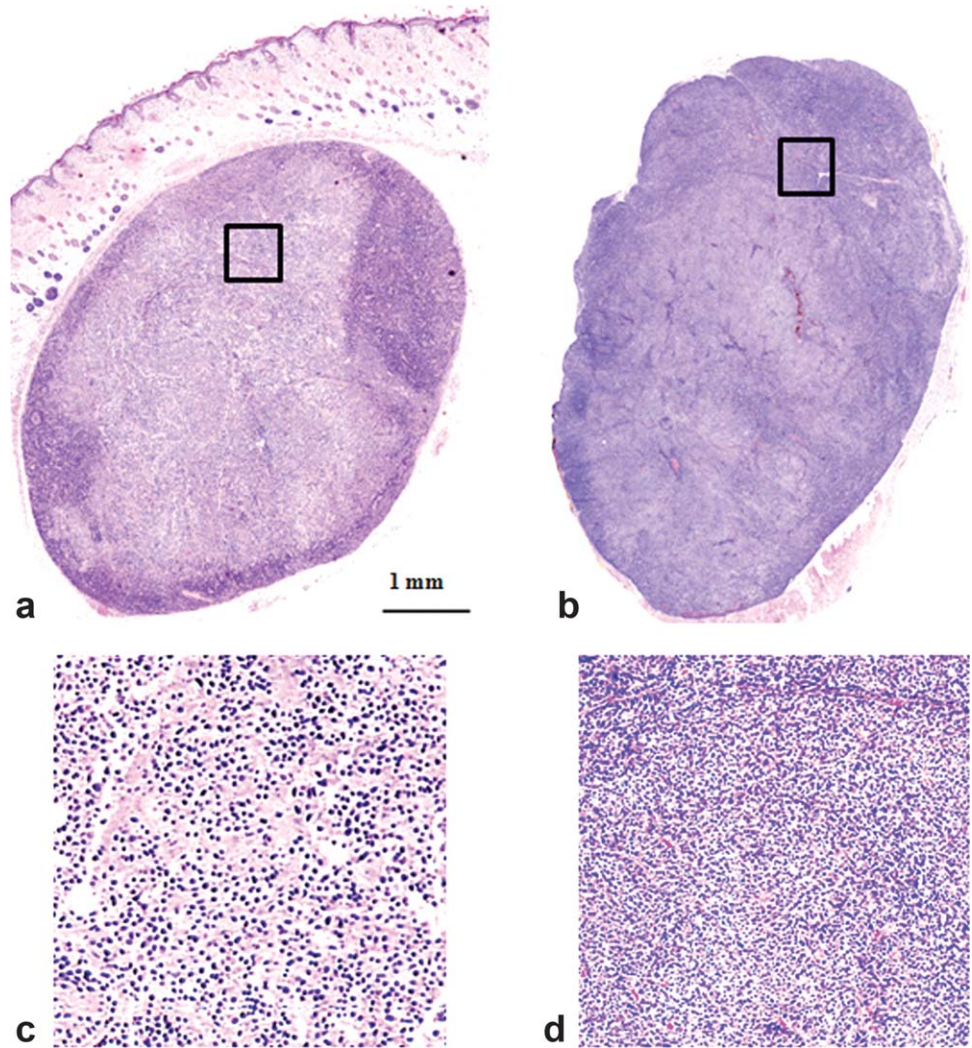


**Figure 7.** Histologic images of treated (left) and control (right) tumors 24 h after PDT. **a:** Treated mouse (M104). **b:** A dark control tumor. Significant morphological difference illustrated the therapeutic effect 24 h after the treatment. The rectangular areas on images (a) and (b) were magnified and shown in images (c) and (d), respectively. Massive areas of tumor cell damage were shown on (c) in comparison with the intact tumor cells in (d).

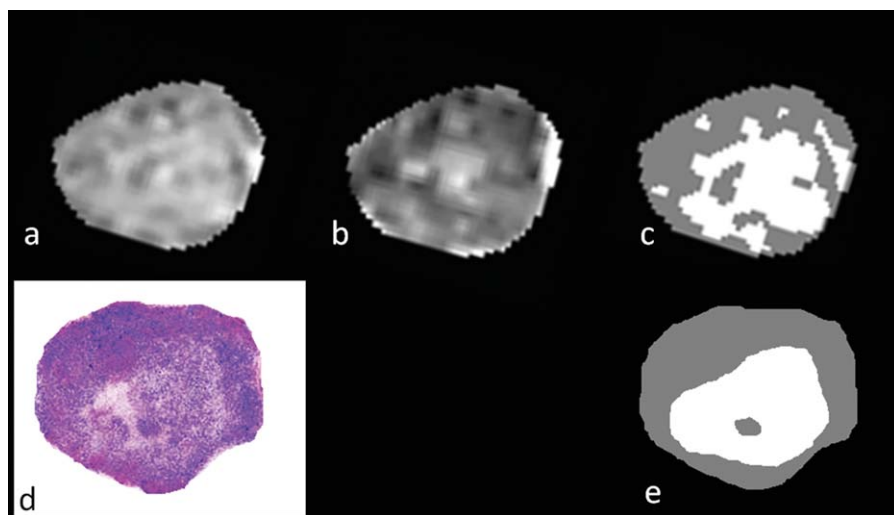


**Figure 8.** Tissue classification of a PDT-treated tumor. **a:** DW-MRI image of a segmented tumor. **b:** The corresponding ADC map. **c:** Classified result where two intensities illustrate the class of each pixel: bright is the necrosis; gray is the viable region; and dark is the image background. **d:** Corresponding histology of the same tumor. **e:** The classification result from the histologic image (d). The two tissue classes (necrotic and viable tumor) on the histologic image correspond to those on the classified result from MRI and ADC map.

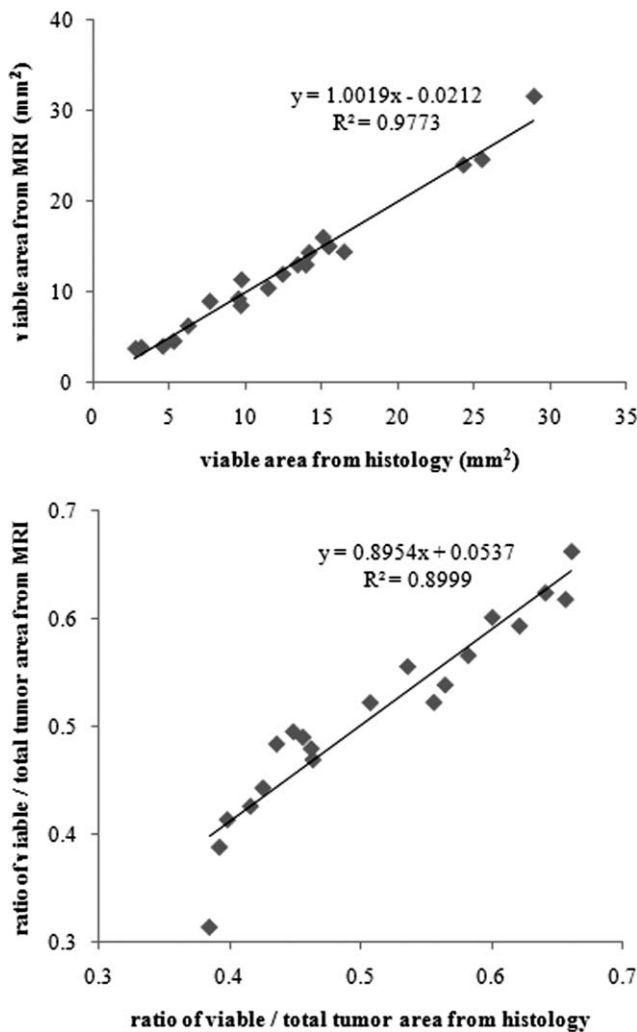


**Figure 9.** Correlation of tumor tissue classification from MR images and histology. Viable tumor area and its proportion to the total tumor were measured on both MR and histology 24 h after PDT. Twenty MR slices and histology from 17 treated tumors are compared. **Top:** The viable area measured by classification of tumor DW-MRI and ADC is as a function of the viable area measured by segmentation of histology. **Bottom:** The viable region ratio measured from MRI is plotted as a function of the ratio from histology.

classifying the tumor into different tissue types and thus potentially improving therapy assessment.

DW-MRI images and ADC maps provide *in vivo* information regarding the water diffusion within the tissue. It has been used to discriminate between healthy and malignant tissue, and assess tumor responses to chemotherapy, irradiation, and gene therapy (28,29). The water diffusion in tissue is restricted by cell membranes and organelles. Therefore, water molecules diffusion indirectly characterizes tissue microenvironment that is associated with cellular integrity and pathologic conditions (29). Note that the diffusion-weighted MRI signal at a voxel is described as  $S = S_0 \exp(-b \cdot ADC)$ . Accordingly, MR intensity inversely depends on the ADC, and a voxel with a high intensity in DW-MRI will have a small value of ADC when a specific  $b$  is used. However, DW-MRI signal depends not

only on water molecule diffusion but also on the signal  $S_0$  that is T2 weighted. Although the edema surrounding the treated tumor 24 h after PDT appears to have similar intensities as the tumor, it shows much higher ADC on the map because edema has a longer T2 value than the tumor (30). As ADC was computed by a function fitting which removed T2 weighted signal effect, ADC map has better contrast differentiation of the tumor from edema, and it may be more reliable to characterize cellular properties than the DW-MRI images.

PDT generates reactive oxygen species that lead to tumor cell injury, vascular damage, and possible immune response. Although the principal mechanism of tumor ablation by Pc 4-PDT has not been completely understood, mitochondrial damage appears to play a major role in cell killing because Pc 4 localizes in cell mitochondria as well as other intracellular organelles (31,32). Therefore, Pc 4-PDT might lead to cell necrosis or apoptosis as the first step of tumor treatment. Tumor necrosis is characterized by massive cell damage, reduced cell density, increased intercellular space, and liberation of water molecules from cell membrane restriction. All the responses cause elevation of water molecule mobility in comparison with the restricted diffusion in viable tumor. This probably results in the increase of diffusion coefficient 24 h after PDT. Our results show that the change in ADC 24 h after therapy is consistent with the tumor necrosis as observed in histology, and it is also consistent with the change in PSA levels 7 days later. The diffusion response of treated tumors probably supports the rule of nonvascular cell injury in the early therapeutic effect of Pc 4-PDT. Diffusion-weighted MRI and ADC have been used to monitor brain tumors under radiation therapy and other treatments (33,34). The present study suggests that the change in tumor ADC values 24 h after treatment may serve as a biomarker of early therapeutic effect of Pc 4-PDT of prostate cancer.

Phase I clinical trials of Pc 4-PDT has been reported for treatment of cutaneous cancers (35). Our study may provide a tool for an early predication of treatment outcome. However, due to the difference of specific tumors, different ADC change should be anticipated when translating the study from mice to human. When the treatment is applied to tumors at different stages, relative ADC change might be more important than absolute values for assessing therapy-induced response. It is likely that time point post-therapy is important for effective treatment monitoring. Our results suggest the potential of DW-MRI as a noninvasive methodology of rapid monitoring tumor response to PDT within 24 h after therapy.

We conclude that diffusion-weighted MRI and ADC measurement can provide a noninvasive imaging marker for assessing early therapeutic effect of Pc 4-PDT in the CWR22 tumor model. The imaging techniques can be useful for monitoring photodynamic therapy of cancer in a clinical setting.

#### ACKNOWLEDGMENTS

The authors thank Dr. Nancy Oleinick for inspiring discussions, Dr. Malcolm Kenney for providing Pc 4,

Joseph Meyers for assistance with animal experiments, Dr. Thomas G. Pretlow and Nancy Edgehouse for the CWR22 cell lines and histologic processing of the tissues.

## REFERENCES

- Triesscheijn M, Baas P, Schellens JH, et al. Photodynamic therapy in oncology. *Oncologist* 2006;11:1034–1044.
- Schneider LA, Hinrichs R, Scharffetter-Kochanek K. Phototherapy and photochemotherapy. *Clin Dermatol* 2008;26:464–476.
- Huang Z, Chen Q, Dole KC, et al. The effect of Tookad-mediated photodynamic ablation of the prostate gland on adjacent tissues—*in vivo* study in a canine model. *Photochem Photobiol Sci* 2007;6:1318–1324.
- Josefsen LB, Boyle RW. Photodynamic therapy and the development of metal-based photosensitisers. *Met Based Drugs* 2008;2008:276109.
- Juarranz A, Jaen P, Sanz-Rodriguez F, et al. Photodynamic therapy of cancer. Basic principles and applications. *Clin Transl Oncol* 2008;10:148–154.
- Fei B, Wang H, Meyers JD, et al. High-field magnetic resonance imaging of the response of human prostate cancer to Pc 4-based photodynamic therapy in an animal model. *Lasers Surg Med* 2007;39:723–730.
- Jiang Q, Knight RA, Chopp M, et al. 1H magnetic resonance imaging of normal brain tissue response to photodynamic therapy. *Neurosurgery* 1991;29:538–546.
- Dodd NJ, Moore JV, Poppitt DG, et al. *In vivo* magnetic resonance imaging of the effects of photodynamic therapy. *Br J Cancer* 1989;60:164–167.
- Liu YH, Hawk RM, Ramaprasad S. *In-vivo* relaxation-time measurements on a murine tumor-model - prolongation of T-1 after photodynamic therapy. *Magn Reson Imaging* 1995;13:251–258.
- Winsborrow BG, Grondy H, Savoie H, et al. Magnetic resonance imaging evaluation of photodynamic therapy-induced hemorrhagic necrosis in the murine M1 tumor model. *Photochem Photobiol* 1997;66:847–852.
- Kennedy SD, Szczepaniak LS, Gibson SL, et al. Quantitative MRI of Gd-Dtpa uptake in tumors - response to photodynamic therapy. *Magn Reson Med* 1994;31:292–301.
- Trachtenberg J, Weersink RA, Davidson SRH, et al. Vascular-targeted photodynamic therapy (padoporfin, WST09) for recurrent prostate cancer after failure of external beam radiotherapy: a study of escalating light doses. *BJU Int* 2008;102:556–562.
- Haider MA, Davidson SR, Kale AV, et al. Prostate gland: MR imaging appearance after vascular targeted photodynamic therapy with palladium-bacteriopheophorbide. *Radiology* 2007;244:196–204.
- Gross S, Gilead A, Scherz A, et al. Monitoring photodynamic therapy of solid tumors online by BOLD-contrast MRI. *Nat Med* 2003;9:1327–1331.
- Bremner JC, Wood SR, Bradley JK, et al. 31P magnetic resonance spectroscopy as a predictor of efficacy in photodynamic therapy using differently charged zinc phthalocyanines. *Br J Cancer* 1999;81:616–621.
- Ramaprasad S, Ripp E, Missert J, et al. *In vivo* 19F MR studies of fluorine labeled photosensitizers in a murine tumor model. *Curr Drug Discov Technol* 2007;4:126–132.
- Plaks V, Koudinova N, Nevo U, et al. Photodynamic therapy of established prostatic adenocarcinoma with TOOKAD: a biphasic apparent diffusion coefficient change as potential early MRI response marker. *Neoplasia* 2004;6:224–233.
- Huang Z, Haider MA, Kraft S, et al. Magnetic resonance imaging correlated with the histopathological effect of Pd-bacteriopheophorbide (Tookad) photodynamic therapy on the normal canine prostate gland. *Lasers Surg Med* 2006;38:672–681.
- Roth Y, Tichler T, Kostenich G, et al. High-b-value diffusion-weighted MR imaging for pretreatment prediction and early monitoring of tumor response to therapy in mice. *Radiology* 2004;232:685–692.
- Fei B, Wang H, Wu C, et al. Choline PET for monitoring early tumor response to photodynamic therapy. *J Nucl Med* 2010;51:130–138.
- Fei B, Wang H, Wu C, et al. Choline molecular imaging with small-animal PET for monitoring tumor cellular response to photodynamic therapy of cancer. *Proc SPIE* 2009;726211.
- Fei B, Wang H, Muzic RF Jr, et al. Deformable and rigid registration of MRI and microPET images for photodynamic therapy of cancer in mice. *Med Phys* 2006;33:753–760.
- Wainstein MA, He F, Robinson D, et al. CWR22: androgen-dependent xenograft model derived from a primary human prostatic carcinoma. *Cancer Res* 1994;54:6049–6052.
- Oleinick NL, Antunez AR, Clay ME, et al. New phthalocyanine photosensitizers for photodynamic therapy. *Photochem Photobiol* 1993;57:242–247.
- Colussi VC, Feyes DK, Mulvihill JW, et al. Phthalocyanine 4 (Pc 4) photodynamic therapy of human OVCAR-3 tumor xenografts. *Photochem Photobiol* 1999;69:236–241.
- Le Bihan D, Breton E, Lallemand D, et al. MR imaging of intravoxel incoherent motions: application to diffusion and perfusion in neurologic disorders. *Radiology* 1986;161:401–407.
- Wang H, Fei B. A modified fuzzy C-means classification method using a multiscale diffusion filtering scheme. *Med Image Anal* 2009;13:193–202.
- Inan N, Arslan A, Akansel G, et al. Diffusion-weighted imaging in the differential diagnosis of cystic lesions of the pancreas. *AJR Am J Roentgenol* 2008;191:1115–1121.
- Charles-Edwards EM, deSouza NM. Diffusion-weighted magnetic resonance imaging and its application to cancer. *Cancer Imaging* 2006;6:135–143.
- Hoehn-Berlage M, Tolxdorff T, Bockhorst K, et al. *In vivo* NMR T2 relaxation of experimental brain tumors in the cat: a multiparameter tissue characterization. *Magn Reson Imaging* 1992;10:935–947.
- Xue LY, Chiu SM, Azizuddin K, et al. The death of human cancer cells following photodynamic therapy: apoptosis competence is necessary for Bcl-2 protection but not for induction of autophagy. *Photochem Photobiol* 2007;83:1016–1023.
- Oleinick NL, Morris RL, Belichenko I. The role of apoptosis in response to photodynamic therapy: what, where, why, and how. *Photochem Photobiol Sci* 2002;1:1–21.
- Cui Y, Zhang XP, Sun YS, et al. Apparent diffusion coefficient: potential imaging biomarker for prediction and early detection of response to chemotherapy in hepatic metastases. *Radiology* 2008;248:894–900.
- Harry VN, Semple SI, Gilbert FJ, et al. Diffusion-weighted magnetic resonance imaging in the early detection of response to chemoradiation in cervical cancer. *Gynecol Oncol* 2008;111:213–220.
- Miller JD, Baron ED, Scull H, et al. Photodynamic therapy with the phthalocyanine photosensitizer Pc 4: the case experience with preclinical mechanistic and early clinical-translational studies. *Toxicol Appl Pharmacol* 2007;224:290–299.

Wang H, Fei BW (corresponding author). Diffusion-weighted MRI for monitoring tumor response to photodynamic therapy. *Journal of Magnetic Resonance Imaging* 2010;32:409-417.

Copyright 2001 Wiley-Liss, Inc. One print or electronic copy may be made for personal use only. Systematic reproduction and distribution, duplication of any material in this paper for a fee or for commercial purposes, or modification of the content of the paper are prohibited.

This paper is publically available in the PubMed Central

<http://www.ncbi.nlm.nih.gov/pubmed/20677270>